Talanta 270 (2024) 125597

Contents lists available at ScienceDirect

Talanta

journal homepage: www.elsevier.com/locate/talanta

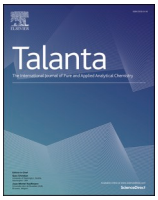

Label-free electrochemical immunosensing of glial fibrillary acidic protein (GFAP) at synthesized rGO/MoS_2/AgNPs nanocomposite. Application to the determination in human cerebrospinal fluid

Lorena García-Rodrigo [1], Claudia Ramos-López [1], Esther Sánchez-Tirado, Lourdes Agüí, Araceli González-Cortés, Paloma Yáñez-Sedeño [*], José M. Pingarrón

Department of Analytical Chemistry, Faculty of Chemistry, University Complutense of Madrid, 28040, Madrid, Spain

ARTICLE INFO

Keywords:
GFAP
Cerebrospinal fluid
Molybdenum disulfide
Reduced graphene oxide
Silver nanoparticles
Electrochemical immunosensor
Label-free

ABSTRACT

An electrochemical bioplatform involving screen-printed carbon electrodes modified with rGO/MoS_2/AgNPs nanocomposites, the covalent immobilization of the specific capture antibody, and label-free detection has been developed for the determination of Glial Fibrillary Acidic Protein (GFAP). The resulting immunosensor profits the benefits of the rGO high conductivity, the pseudo-peroxidase activity of MoS_2 and the electrocatalytic effect provided by AgNPs for improving the reduction current responses of hydrogen peroxide at the electrode surface. GFAP is a biomarker of central nervous system injuries has been proposed for the detection and monitoring of neurological diseases as epilepsy, encephalitis, or multiple sclerosis. For the first time, amperometric detection of the immunosensing event was performed by measuring the electrocatalytic response of hydrogen peroxide reduction at the modified electrode. Several techniques including scanning (SEM) and transmission (TEM) electron microscopies were used for the characterization of the synthesized composite whilst electrochemical impedance spectroscopy (EIS) using the redox probe $Fe(CN)_6^{3-/4-}$ was employed to evaluate the success of the steps implied in the fabrication of the immunosensor. After optimization of the involved experimental variables, a linear calibration plot for GFAP was constructed over the 0.6–100 ng mL^{-1} range, and a detection limit of 0.16 ng mL^{-1} was achieved. The developed immunosensor was successfully applied to the determination of GFAP in human cerebrospinal fluid (CSF) of patients diagnosed with encephalitis.

1. Introduction

Glial Fibrillary Acidic Protein (GFAP) is an intermediate filament protein expressed in astrocytes and involved in their structural roles and functions during regeneration, synaptic plasticity, and reactive gliosis [1]. Although this protein is typically not detectable in the plasma of healthy individuals, increased levels can be found in the cerebrospinal fluid (CSF) and in the serum of patients with neurodegenerative disorders brain tumours or cerebrovascular events. Blood GFAP has been defined as an emerging biomarker in brain and spinal cord disorders [2], where variations in the protein concentration are considered as a marker of central nervous system injuries. More specifically, the serum contents of this protein are significantly higher in patients with epileptic seizures [3] and early multiple sclerosis (MS) [4]. The expression of GFAP has been claimed to be indicative of the subtype and degree of progression of these diseases.

Since, in 2018, the FDA authorized a panel test for blood-derived brain protein biomarkers, including GFAP, for clinical use in monitoring of neurological disorders [2], the development of methods for the determination of this protein with application in the diagnosis and follow-up of such diseases has grown rapidly. However, several challenges to overcome are related to the low levels of GFAP in biological samples, as well as to the small differences between GFAP concentrations found in patients with neurological diseases and healthy individuals as well as the increase with age in the GFAP levels in the latter group. For instance, in the case of epilepsy, mean GFAP concentrations in the serum of patients with epileptic seizures have been found to be around 3.7 ng mL^{-1}, which are only slightly higher than the cut-off value set at 2.7 ng mL^{-1} [3]. Regarding MS, the mean levels of GFAP in the serum of patients with secondary or primary progressive multiple

* Corresponding author.
E-mail address: yseo@quim.ucm.es (P. Yáñez-Sedeño).
[1] These authors have equally contributed to this work.

https://doi.org/10.1016/j.talanta.2023.125597
Received 3 November 2023; Received in revised form 21 December 2023; Accepted 22 December 2023
Available online 23 December 2023

sclerosis (SPMS or PPMS, respectively) are around 146 pg mL^{-1} and 130 pg mL^{-1} respectively, with a mean level in healthy individuals of 92 pg mL^{-1}. However, these concentrations are much higher in CSF samples, where the GFAP mean levels are 12.3 ng mL^{-1} and 10.3 ng mL^{-1}, for MS patients, respectively [4]. In addition, a mean value of 38.0 ng mL^{-1} GFAP in CSF was reported for patients diagnosed with encephalitis [5].

ELISA and SIMOA® technologies have been mainly used for the determination of GFAP in biological samples. The commercial ELISA kits available for this protein are mostly based on sandwich-type immunoassays using biotinylated detection antibodies and peroxidase conjugates with streptavidin or avidin. For example, the Millipore test (NS830 GFAP ELISA) [www.merckmillipore.com/ES/es/product/GFAP-ELISA-Kit, MM_NF-NS830] provides a linear calibration plot from 1.5 to 100 ng mL^{-1} GFAP, requiring an assay time of 3.5 h. The Mybiosource kit (ELISA kit No MBS704044) [www.mybiosource.com/gfap-human-elisa-kits/glial-fibrillary-acidic-protein/704044], with the same assay time and working at 37 °C, provides a semi-log calibration for GFAP between 0.625 and 40 ng mL^{-1}. Finally, the R&D Systems ELISA kit [www.rndsystems.com/products/human-gfap-duoset-elisa_dy2594-05] needs a longer assay time of 4 h 40 min at room temperature and provides a semi-logarithmic calibration between 0.3 and 20 ng mL^{-1} GFAP. On the other hand, SIMOA® technology, based on digital single molecule measurements, has a higher sensitivity. For instance, the Simoa™ GFAP Discovery Kit from Quanterix [www.quanterix.com/simoa-assay-kits/gfap/] allows a semi-log calibration with a dynamic range from 1.37 pg mL^{-1} (lower limit of quantification) to 1 ng mL^{-1}.

Regarding biosensors, few examples of electrochemical immunoplatforms for the determination of GFAP have been reported. An impedimetric label-free immunosensor involving branched polyethylenimine (PEI) adsorbed onto graphene surfaces was developed and applied to spiked serum and artificial CSF [6]. Using $[Fe(CN)_6]^{3-/4-}$ as the redox probe, a semilogarithmic calibration plot with a linear range between 1 and 10^5 pg mL^{-1} GFAP was claimed. More recently, another impedimetric label-free design involving a hybrid graphene nanosheet intermixed poly(3,4-ethylenedioxythiophene) polystyrene sulfonate (PEDOT: PSS) embedded within the base carbon matrix (GiPEC) of a screen-printing ink was reported. The linear range was from 1 pg mL^{-1} to 10 ng mL^{-1} and the immunosensor was applied in spiked serum [7]. Zeolitic imidazolate frameworks and reduced graphene oxide anchored with gold nanoparticles (Au@ZIF-8@rGO) were also used for the impedimetric determination of GFAP in spiked urine achieving a linear calibration plot from 50.0 to 10^4 fg mL^{-1} [8]. Covalent immobilization of anti-GFAP antibodies onto L-cysteine/gold nanoparticles was also used for the development of a label-free impedimetric immunosensor for GFAP over the 1.0–1000.0 pg mL^{-1} range and application to spiked synthetic serum [9]. More recently, Ozcelikay et al. prepared an electrochemical immunoplatform involving magnetic microbeads for the sandwich-type immunosensing of GFAP using a biotinylated detector antibody and streptavidin-peroxidase conjugates. Amperometric transduction of the hydrogen peroxide/hydroquinone system provided a linear calibration plot over the range between 0.24 and 31.6 ng mL^{-1} GFAP [10].

As it can be deduced, practically all immunosensors developed to date for the determination of GFAP involved label-free detection with impedimetric transduction, but validation was performed only with spiked and artificial samples. In general, label-free biosensors enable simplified and reagentless measurements providing increased scope for commercial exploitation [11]. However, usually, non-specific adsorption on the corresponding support may be observed thus producing significant effect on the responses by reducing sensitivity and then requiring the use of proper surface blockers. Particularly, impedimetric immunosensors exhibit low detection limits but often suffer from low reproducibility, especially in the determination of small molecules and the analysis of real samples which are far more complex than spiked or artificial samples. In addition, on-site applications are hampered by the need to match them with a suitable metric device [12]. In this context, we report in this paper the label-free amperometric determination of GFAP taking advantage of the electrocatalytic and synergic action of a synthesized nanocomposite combining rGO, MoS_2 and AgNPs, which allows the sensitive and selective determination of the protein in real clinical samples.

Among the nanomaterials used for the preparation of the modified electrode, MoS_2 is a representative of two-dimensional (2D) transition metal dichalcogenides (TMDs) which has been widely used in bioelectronics, including (bio)sensing because of its biocompatibility and semiconductivity [13]. One of the main applications of MoS_2 derives from its intrinsic peroxidase-like catalytic activity [14]. Indeed, the electrocatalytic effect towards the electrochemical reduction of hydrogen peroxide provides sensitive responses with the advantage of a high selectivity, since interferences by oxidizable compounds such as ascorbic acid (AA), uric acid (UA) or dopamine (DA), usually present in clinical samples, are avoided [15]. Several electrochemical biosensors have been reported using MoS_2 nanoparticles [16], nanosheets [17] or quantum dots [18]. However, in most cases, MoS_2 hybrids or composites with carbon nanomaterials have been employed to minimize the relatively low electrical conductivity and easy aggregation of MoS_2. The combination with graphene or carbon nanotubes with high surface area and electronic conductivity has demonstrated to be a good alternative to prepare nanocomposites that increased the electrocatalytic efficiency and conductivity of MoS_2 [19]. Furthermore, the incorporation of metallic nanoparticles into MoS_2 hybrids not only leads to improved physicochemical properties but also enhances the stability. Silver nanoparticles (AgNPs), due to the advantages of low cost, good electrical conductivity and high electrocatalytic activity, have been combined with MoS_2 and graphene to prepare electrochemical biosensors applied, for example, to the determination of carcinoembryonic antigen (CEA) [20]. Very recently, an aptasensor for the determination of Troponin I was prepared involving green lignin-derived graphene with MoS_2 and embedded AgNPs to improve the interaction between the aptamer and the target biomarker [21].

In this work, a nanocomposite prepared with rGO and MoS_2 decorated with AgNPs was synthesized to be used as a modifier of carbon screen-printed electrodes (SPCEs) for the further development of an amperometric label-free immunosensor for the determination of GFAP. The strategy involved covalent immobilization of the specific capture antibody (anti-GFAP), conjugation with the antigen (GFAP) and direct detection of the immunosensing event by measuring the electrocatalytic response of hydrogen peroxide reduction at the modified electrode. The synthesis of the composite, and the characterization of the steps involved in the preparation of the immunosensor allowed the development of a method for the determination of GFAP in a 0.6–100 ng mL^{-1} linear range with a limit of detection of 0.16 ng mL^{-1}. The proposed immunosensor was successfully applied to the determination of GFAP in human cerebrospinal fluid (CSF) of patients diagnosed with encephalitis and the results were validated by comparison with those obtained using an ELISA method.

2. Experimental

2.1. Apparatus and electrodes

Amperometric measurements were made at room temperature using a CH1 1030B potentiostat (Chemical Instruments, Inc.) controlled by the CH1 1030B software. A μAutolab type III potentiostat (Ecochemie) controlled by FRA2 software electrochemical impedance spectroscopy (EIS) was employed for other electrochemical measurements. Screen-printed carbon electrodes (SPCEs, DRP-110) with a 4 mm-Ø carbon working electrode (Metrohm-DropSens) including a carbon counter electrode and a silver pseudo-reference electrode were used. The specific DRP-CAC connection cables employed as interface between the SPCEs and the potentiostat were also from Metrohm-Dropsens. Regarding characterization studies by CV and EIS, the measurements were

performed in stirred solutions using 10-mL glass electrochemical cells from Pobel.

A Crison model Basic 20 + pH meter, a P-Selecta Ultrasons ultrasonic bath, a Heidolph Reax Top homogenizer for small samples, and an MPW-65R centrifuge from MPW (Med. Instruments) were also used. ELISA absorbance readings were made using a Sunrise™ Tecan microplate reader with the Magellan V 7.1 software.

Scanning electron microscopy (SEM) was made using a field emission scanning electron microscope (JSM 7600F) with an accelerating voltage of 5 kV and 8 mm working distance, equipped with the energy dispersive X-ray (EDX) spectrometer, with 133 eV resolution. The synthesized nanomaterial was deposited as a powder on a carbon ribbon onto the support placed in the sample holder of the equipment. Transmission electron microscopy (TEM) was performed using a JEM 2100 PLUS microscope equipped with a thermionic cathode electron gun with LaB6 filament, operating at 100 kV, and an Oxford X-Max SDD detector with 129 eV resolution and 80 mm^2 area. A suspension of the nanomaterial, previously dispersed in butanol, with the aid of ultrasound, was deposited on a copper grid in the sample holder.

2.2. Reagents, solutions, and samples

Graphene oxide (NIT.GO.M.140.10) from Nanoinnova Technologies and silver nitrate ($AgNO_3$) from Probus, were used. Sodium molybdate ($Na_2MoO_4{\cdot}2H_2O$), trisodium citrate ($Na_3C_3H_5O(COO)_3$), sodium borohydride ($NaBH_4$) and thiourea (CH_4N_2S), all from Sigma-Aldrich, were also used. Human GFAP capture antibody (anti-GFAP) and human GFAP antigen were obtained from the GFAP ELISA kit SEA068Hu from Cloud-Clone Corp. Polyoxyethylene (20) sorbitan monolaurate (Tween 20), *N*-(3-dimethylamino-propyl)-*N*′-ethylcarbodiimide (EDC), sodium *N*-hydroxysulfo-succini-mide (sulfo-NHS) and hydrogen peroxide (H_2O_2, 30% v/v), were from Sigma-Aldrich. The blocking solution used was a commercial Blocker™ from Thermo Fisher Scientific consisting of 1% w/v casein in PBS. Buffer solutions were: 25 mM MES of pH 5.0 prepared from 2-(*N*-morpholine) ethano-sulfonic acid (Gerbu); 100 mM and 50 mM pH 6.0 phosphate buffers (PB) prepared from Na_2HPO_4 and $NaH_2PO_4{\cdot}2H_2O$ (Sigma-Aldrich); phosphate saline buffers (PBS), consisting of a 100 mM sodium phosphate buffer of pH 7.4 supplemented with 2.0 g NaCl and 50.25 mg KCl (Scharlab) in 250 mL deionized water. In all cases, the pH value was adjusted by adding the required volume of 2 M NaOH solution. Deionized water was from a Millipore Milli-Q purification system (18.2 MΩ cm). The analyzed samples were purchased in Central BioHub® GmbH, Hennigsdorf, Germany, and consisted of CSF from patients diagnosed with encephalitis. GFAP was determined with the immunosensor without sample treatment and the obtained results were compared with those provided by the SEA068Hu ELISA kit from Cloud-Clone Corp. for 20-fold diluted CSF samples. All the experiments were performed accomplishing all the ethical issues and relevant guidelines and regulations of the involved institution.

2.3. Procedures

2.3.1. Synthesis of rGO/MoS_2

The method described by Li et al. [18,22] with slight modifications was employed for the synthesis of rGO/MoS_2 hybrids. Briefly, 0.4 g $Na_2MoO_4{\cdot}2H_2O$ were added to 30 mg GO dispersed in 30 mL of water and the mixture was ultrasonically stirred for 10 min. Then, 0.63 g urea were added, and the solution was sonicated for other 30 min. Thereafter, the reaction solution was transferred to a 50-mL Teflon-lined autoclave and heated in an oven at 200 °C for 24 h. Then, the mixture was cooled at room temperature, and the product was collected by centrifugation at 6000 rpm for 6 min, washed four times with deionized water and ethanol, and vacuum-dried at 60 °C.

2.3.2. Synthesis of AgNPs

The method reported by Wan et al. [23] was used for the synthesis of AgNPs. A solution of 0.2 g of trisodium citrate in 95 mL of water was prepared by heating at 70 °C for 15 min. Then, 1.7 mL of a 10 mg mL^{-1} $AgNO_3$ solution were added followed by the immediate addition of 2 mL of a freshly prepared 1 mg mL^{-1} $NaBH_4$ solution. The mixture was kept at 70 °C for 1 h under vigorous stirring. The colour of the solution changed to a bright yellowish-brown indicating the formation of silver seeds. Separately, 2 mL of a 10 mg mL^{-1} citrate solution and 80 mL of water were transferred to a round bottom flask, heated to the boil and maintained for 15 min. Subsequently, 10 mL of the as prepared Ag seeds solution and 1.7 mL of 10 mg mL^{-1} $AgNO_3$ solution were successively added to the mixture and kept during 1 h at reflux. The resulting solution turned bright golden yellow, indicating that the AgNPs were formed.

2.3.3. Synthesis of rGO/MoS_2/AgNPs

20 mg of the as prepared rGO/MoS_2 were added to 20 mL of AgNPs and the mixture was shaken for 12 h at room temperature [20]. Then, the resulting product was washed four times with deionized water and vacuum-dried at 60 °C.

2.3.4. Preparation of the immunosensor

The scheme depicted in Fig. 1 shows the steps involved in the modification of the SPCE, the preparation of the immunosensor, and the electrochemical detection. Once the rGO/MoS_2/AgNPs composite was synthesized, a 3 μL aliquot of a 2 mg mL^{-1} dispersion in 0.05% (w/v) Tween 20 was deposited on the SPCE surface allowing it to dry at room temperature. Next, the electrode was washed with deionized water allowing drying again, and 10 μL of a 0.1 mol L^{-1} EDC/sulfo-NHS solution prepared in 25 mM MES buffer of pH 5.0 were added and incubated for 30 min in a humid ambient at room temperature. The electrode was washed with the same MES buffer solution. The capture antibody (anti-GFAP) was covalently immobilized on the activated rGO/MoS_2/AgNPs/SPCE by dropping 5 μL of a 4 μg mL^{-1} anti-GFAP solution and incubating overnight in humid environment at 4 °C. After washing with PBS of pH 7.4, the unreacted activated groups of the anti-GFAP-rGO/MoS_2/AgNPs/SPCE were blocked by adding 5 μL of 1% (w/v) casein in PBS (Blocking Buffer™) allowing incubation for 60 min. Thereafter, the electrode was washed with PBS pH 7.4.

2.3.5. Amperometric detection

The target protein was conjugated to the capture antibody by adding 5 μL of the GFAP standard solution (or the sample), incubating for 90 min, and washing with PBS pH 7.4. Amperometric measurements were performed by depositing 45 μL of 100 mM PBS pH 6.8 onto the surface of the horizontally positioned GFAP-anti-GFAP-rGO/MoS_2/AgNPs/SPCE and by applying a potential of −0.40 V vs Ag pseudo-reference electrode. Then, 5 μL of a 50 mM H_2O_2 prepared in the same buffer were added and, upon current stabilization (approximately 100 s), the variation of cathodic response occurring by the electrochemical reduction of H_2O_2 at the electrode surface was measured. Amperometric signals were calculated as the difference between such steady state currents and the background currents. The given values are the mean value of three replicates, and the error bars were estimated as three times the standard deviation of each set of replicates ($\alpha = 0.05$).

2.3.6. Analysis of CSF samples

The developed immunosensor was applied to the analysis of CSF samples from patients diagnosed with encephalitis which were purchased in Central BioHub® GmbH, Hennigsdorf, Germany and stored at −80 °C until use. All the experiments involved in the samples manipulation and the analysis were performed accomplishing all the ethical issues and relevant guidelines and regulations of the implied institutions. Undiluted CSF was used for the determination of endogenous GFAP, and the results were compared with those provided by an ELISA kit using similar reagents and applied to 20-fold diluted CSF samples. The standards additions method by constructing a calibration plot through the addition of a GFAP standard solutions to sample aliquots

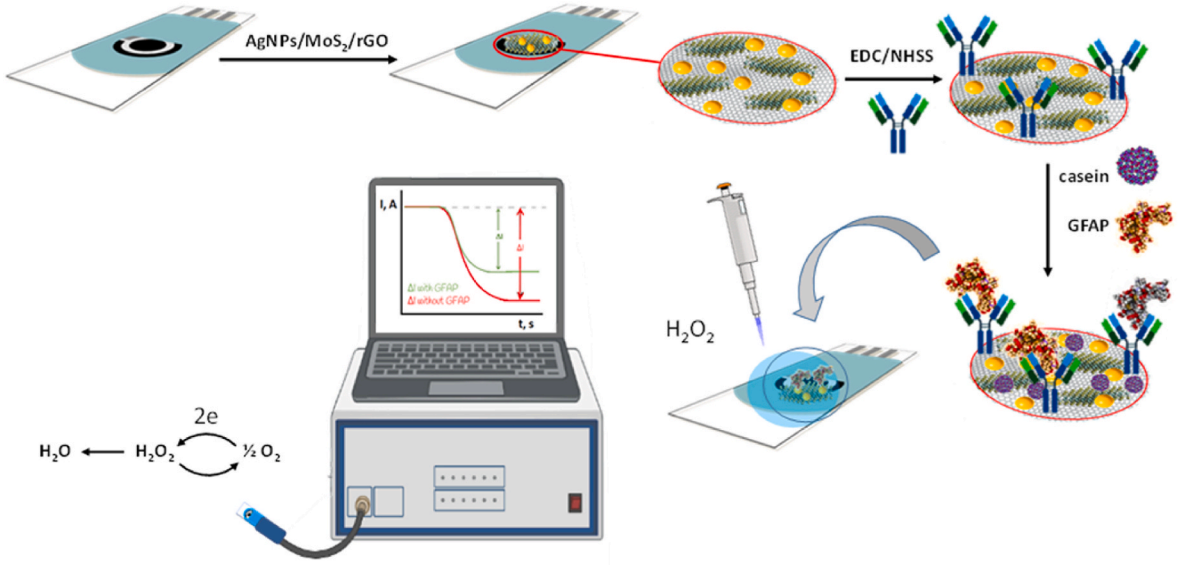

Fig. 1. Scheme displaying the steps involved in the preparation of the label-free amperometric GFAP-anti-GFAP-rGO/MoS_2/AgNPs/SPCE immunosensor as well as the reactions involved in the electrochemical detection.

was employed for target quantification.

3. Results and discussion

As described in the Experimental section, in this work, a label-free amperometric immunosensor for the determination of GFAP was prepared by covalent immobilization of specific anti-GFAP capture antibodies on the surface of a SPCE modified with rGO/MoS_2/AgNPs nanocomposite (Fig. 1). The measurements of the electrocatalytic responses of H_2O_2 at the electrode by applying a −0.40 mV vs Ag pseudo-reference electrode detection potential were inversely dependent on protein concentration. Fig. 1 also shows the reactions responsible of the electrochemical detection involving the electrocatalytic reduction of H_2O_2 on silver nanoparticles at neutral medium [24].

3.1. Characterization studies

The morphology of the synthesized composite was characterized by scanning electron microscopy (SEM). Two SEM images at different magnification levels (Fig. 2A) show a large amount of the hydrothermally synthesized MoS_2 deposited onto rGO as well-dispersed sheets tightly stacked together. Fig. 2B shows the SEM image of rGO/MoS_2/AgNPs with a rough surface morphology in the form of nanoaggregates.

Transmission electron microscopy (TEM) was also used to investigate the structure of MoS_2 nanocomposites. As Fig. 3A shows, MoS_2 nanosheets appear scattered onto rGO sheets. It has been reported that rGO/MoS_2 composites can acquire a 3D architecture caused by self-assembling during the hydrothermal process, in which the reduction of GO can drive to partial overlapping or coalescing of the sheets [25, 26].

Fig. 3B shows some nanoparticles incorporated to the structure of rGO/MoS_2 thus demonstrating the successful preparation of rGO/MoS_2/AgNPs. In addition, the structure of the synthesized AgNPs, with diameters ranging between 15 and 20 nm, is shown in Fig. 3C. EDX spectrum of rGO/MoS_2/AgNPs (Fig. 3D) revealed that the elements C, O, S, Mo and Ag are present in the synthesized nanomaterial, thus confirming the efficiency of the nanocomposite synthesis method. The Cu peaks comes from the used grid.

The electrochemical characterization of the modified SPCEs was performed by dropping 4 μL of the prepared dispersion of rGO/MoS_2/AgNPs onto the electrode surface and allowing drying. Then, cyclic voltammograms (CVs) and electrochemical impedance spectra (EIS) of 5 mM $Fe(CN)_6^{3-/4-}$ solutions prepared in 10 mM PBS of pH 7.4 were recorded and compared with those obtained at the bare electrode, the rGO/SPCE and the rGO/MoS_2/SPCE modified electrodes. As expected, Fig. 4A shows as the rGO/SPCE electrode (curve b) provided the best defined voltammetric response, with the characteristic oxidation and reduction peaks of the redox pair showing larger peak currents (ipa = ipc ~ 157 μA) and ΔE = 150 mV. On the other hand, the voltammograms obtained at the electrodes modified with rGO/MoS_2 (curve c) and

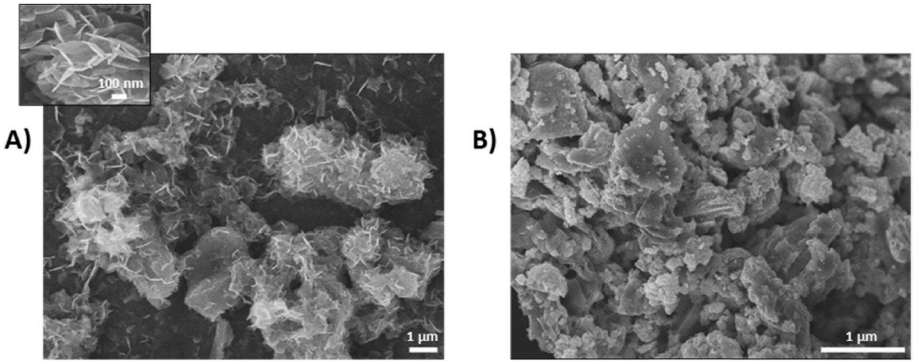

Fig. 2. SEM images of (A) rGO/MoS_2 (inset at higher magnification), (B) rGO/MoS_2/AgNPs.

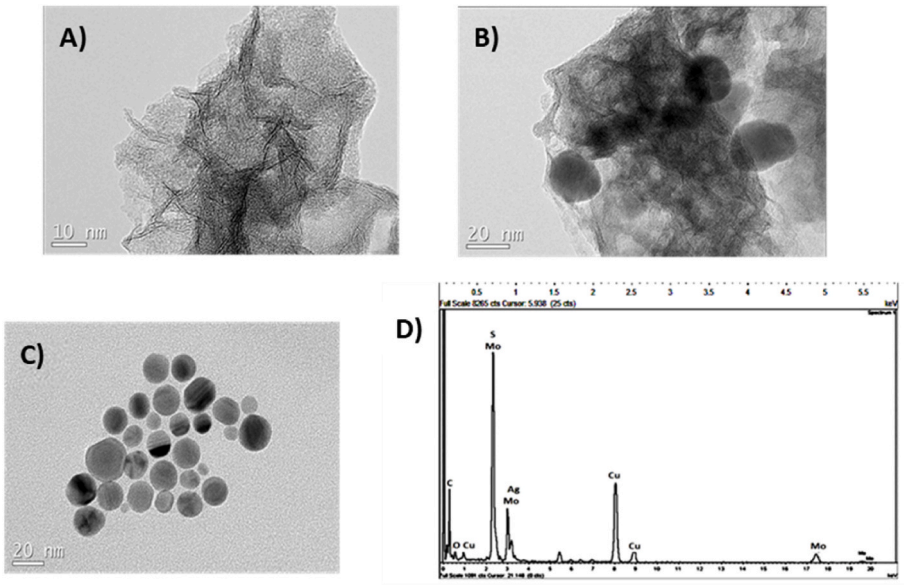

Fig. 3. A–C: TEM images of rGO/MoS_2 (A), rGO/MoS_2/AgNPs (B), AgNPs (C). EDX spectrum of rGO/MoS_2/AgNPs (D).

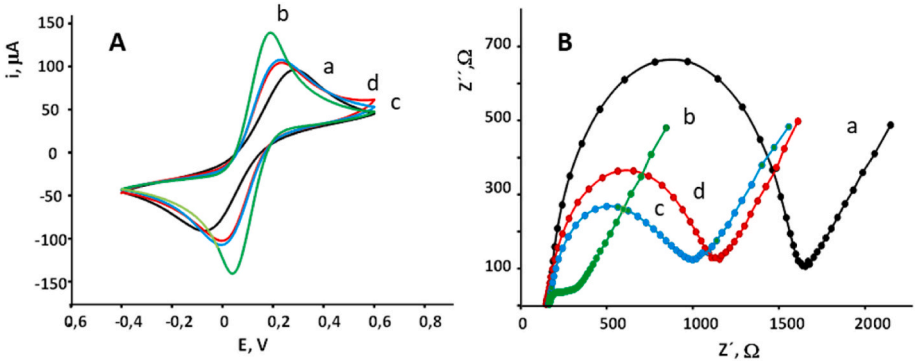

Fig. 4. Cyclic voltammograms (A) and Nyquist plots (B) recorded in 5 mM $Fe(CN)_6^{3-/4-}$ in 10 mM PBS of pH 7.4 at: SPCE (a, black); rGO/SPCE (b, green); rGO/MoS_2/SPCE (c, blue); rGO/MoS_2/AgNPs/SPCE (d, red).

rGO/MoS_2/AgNPs (curve d) are very similar, with lower peak currents (ipa = ipc ~ 107 µA) and a slightly higher ΔE value (230 mV). These results evidenced a lower conductivity of the surfaces modified with these materials compared to the electrode modified with rGO. Since MoS_2 is a semiconductor, it hindered the electron transfer at the electrode surface. Although the presence of AgNPs on the rGO/MoS_2 surface should improve the electron transfer, probably, since these nanoparticles are capped by citrate ions, there was an electrostatic repulsion effect towards the anionic redox probe at the working pH. Nevertheless, the responses on both modified electrodes were better than that observed at the bare electrode, with smaller peak currents (ipa = ipc ~ 96 µA) and ΔE = 350 mV.

Fig. 4B shows the impedance spectra recorded at these same electrodes under the same experimental conditions. As it can be seen, the

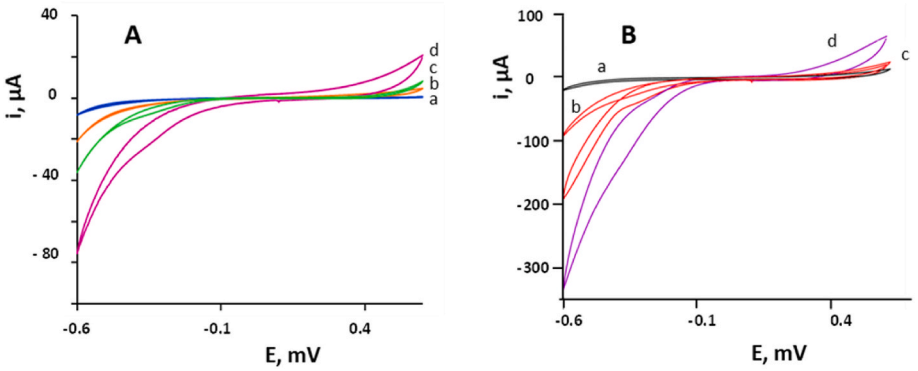

Fig. 5. Cyclic voltammograms in 10 mM PBS pH 7.4 of: (A) 5 mM H_2O_2 at SPCE (a, blue); rGO/SPCE (b, orange); rGO/MoS_2/SPCE (c, green); rGO/MoS_2/AgNPs/SPCE (d, purple). (B) 0 mM H_2O_2 (a, black); 5 mM H_2O_2 (b, red); 10 mM H_2O_2 (c, orange); 20 mM H_2O_2 (d, purple) at rGO/MoS_2/AgNPs/SPCE.

results agreed with those obtained by CV. The resistance to charge transfer is much larger at the bare SPCE, with R_{CT} = 1415 Ω (curve a), that observed at the electrode modified with rGO (curve b), R_{CT} = 95 Ω. Furthermore, the Nyquist curves at rGO/MoS_2/SPCE and rGO/MoS_2/AgNPs/SPCE electrodes (curves c and d) provided R_{CT} values of 732 and 943 Ω, respectively.

With the aim of evaluating the electrochemical behaviour of the modified electrodes towards H_2O_2 which was used as the redox probe for the detection of GFAP, cyclic voltammograms for H_2O_2 were recorded (Fig. 5). As it can be observed, Fig. 5A shows a slight cathodic response in the reductive scan obtained at the rGO/MoS_2/SPCE (curve c), which is not observed at the SPCE (curve a) nor at the rGO/SPCE (curve b). This behaviour is probably due to the pseudo-peroxidase activity of MoS_2 [27], confirming the suitability of this nanomaterial for the electrocatalytic reduction of H_2O_2. In addition, a larger voltammetric response was observed at the rGO/MoS_2/AgNPs/SPCE (curve d), thus showing the relevant role of AgNPs for the electrochemical reduction of H_2O_2. Indeed, this effect has been previously observed by Compton et al. on a silver nanoparticles-modified boron doped diamond electrode in a neutral solution [24]. The authors proposed a CE mechanism involving disproportionation of H_2O_2 to water and oxygen which is further electrochemically reduced to H_2O_2 (see the scheme in Fig. 1) at the AgNPs. The good behaviour of the rGO/MoS_2/AgNPs/SPCE surface towards the electrochemical reduction of H_2O_2 was also deduced form the results displayed in Fig. 5B which showed an increase in the cathodic current as the H_2O_2 concentration increased. These results supported the suitability of the modified electrode for the detection of the redox probe used for the preparation of the immunosensor. Moreover, from these results, a potential value of −0.40 V vs Ag pseudo-reference electrode was selected for the amperometric detection.

3.2. Optimization of the experimental variables involved in the preparation of the immunosensor

According to the scheme shown in Fig. 1, the modified SPCEs were prepared by depositing an aliquot of the rGO/MoS_2/AgNPs dispersion on the electrode surface. After drying and washing, the carboxylic groups on the rGO were activated with the EDC/sulfo-NHS system for further immobilization of the anti-GFAP capture antibody. The effect of the variables implied in the preparation and functioning of the anti-GFAP-rGO/MoS_2/AgNPs/SPCE immunosensor was checked. As it was stated above, the immunosensor responses obtained by addition of H_2O_2 were inversely dependent on the GFAP concentration since as the protein loading at the electrode surface was larger, the measured amperometric current was smaller. Therefore, the selection criterion to optimize each tested variable was a larger ratio between the currents measured with the prepared immunosensor in the absence (B) or in the presence (S) of 50 ng mL^{-1} GFAP standards. The optimization studies implied the evaluation of the rGO/MoS_2/AgNPs suspension volume onto the SPCE surface; the loading and the incubation time of anti-GFAP on the rGO/MoS_2/AgNPs/SPCEs; the type, concentration, and incubation time of the blocking agent; and the incubation time of GFAP protein onto anti-GFAP-rGO/MoS_2/AgNPs/SPCEs. The obtained results are shown in Figs. S1A–E, in the Supplementary Information, and summarized in Table 1.

The step by step preparation of the immunosensor was monitored by EIS and CV. Fig. 6A shows the Nyquist plots recorded in a 5 mM Fe $(CN)_6^{3-/4-}$ solution in 10 mM PBS of pH 7.4, as well as the equivalent circuits used to fit the spectra. As expected, rGO/MoS_2/AgNPs/SPCEs (curve a) exhibited a larger charge transfer resistance (R_{CT} = 943 Ω) than that observed at the same electrode after treatment with EDC/sulfo-NHS (curve b), with R_{CT} = 298 Ω, probably because of the citrate charges neutralization. Interestingly, the presence of the biomolecules at the electrode surface (curves c-e) provoked the appearance of two semicircles in the EIS spectra, Due to the insulating nature of the reagents, successive increases in the second semicircle diameter were

Table 1
Optimization of the experimental variables affecting the preparation and functioning of the anti-GFAP-rGO/MoS_2/AgNPs immunosensor.

Variable	Tested range	Selected value
Volume of rGO/MoS_2/AgNPs, μL	2–7	3
Loading of anti-GFAP, μg mL^{-1}	2–25	4
Immobilization time of anti-GFAP, min	30–150, overnight	overnight
Type and loading of blocking agent	1% w/v casein (BB*), 2% w/v casein, 0.25–2% BSA	1% w/v casein (BB*)
Immobilization time of blocking agent, min	30–90	60
Immobilization time of GFAP protein, min	30–120	90

* Blocking buffer.

observed when anti-GFAP (curve c), the blocking buffer (curve d), and GFAP (curve e) were sequentially incorporated to the electrode, with R_{CT} values of 1136 Ω, 1410 Ω and 1925 Ω respectively. The respective R_{CT} values measured for the smaller semicircles were of 397 Ω, 355 Ω and 162 Ω. These results led to define the obtained Nyquist plots by two different equivalent circuits as shown in Fig. 6A. Curves a and b fitted well to a Randles R1(C2[R3W1]) circuit, whereas curves c, d and e should be explained by the more complex equivalent circuit depicted on the right, with at least two RC semicircuits, reflecting that some parts of the electrode are coated by the biomolecules while others remain exposed to the solution. The parallel RC circuits mean that there is a film with defects such as pinholes or a non-uniform thickness throughout the substrate [28].

Regarding cyclic voltammograms, the results shown in Fig. 6B partially agree with those observed by EIS. As it can be seen, rGO/MoS_2/AgNPs/SPCE (curve a) provided lower peak currents (ipa = ipc ~ 71 μA) than those measured after pretreatment with EDC/NHSS (curve b), with (ipa = ipc ~ 127 μA). The incorporation of biomolecules to the electrode gave rise to a worse definition of the voltammograms, with lower peak currents and no significant voltammetric differences between the electrodes prepared with the antibody, the blocking buffer, and the protein (curves c, d and e, respectively), showing similar anodic and cathodic ip, Ep and ΔE in the electroactivity range of the redox probe. For instance, the GFAP-anti-GFAP-rGO/MoS_2/AgNPs/SPCE immunosensor (curve e) provided ipa = ipc ~ 60 μA, similar to the peak currents measured in the absence of biomolecules. Furthermore, as it can also be observed, the CV oxidation peak measured at the GFAP-anti-GFAP-rGO/MoS_2/AgNPs/SPCE immunosensor appears distorted. This behaviour was also observed in the CV electrochemical responses for other immunosensors involving nanomaterials [29] including MoS_2 [30] and is attributed to the non-conductive nature of immobilized proteins, thus hamptering the electron flow, resulting in a lower electrocatalytic ability of the modified electrode [30]. Once the antibody-antigen locking took place, a thick interlayer is formed at the interface this hindering the redox response. Therefore, the electrodes can exhibit suppression but also dislocation of the redox peaks [29].The larger differences observed using EIS compared with CV are probably due to the different rationale and mode of application of the two techniques. Whereas CV involves large potential perturbations, impedimetric measurements require that the systems are only infinitesimally perturbed with respect to the steady state [31].

3.3. Analytical figures of merit of the immunosensor

Fig. 7 shows the calibration plot constructed with the anti-GFAP-rGO/MoS_2/AgNPs immunosensor as well as some of the recorded amperometric traces. The calibration equation is: i, μA = (−0.069 ± 0.001) [GFAP, ng mL^{-1}] + (9.32 ± 0.04) μA, with a linear interval ranging from 0.5 to 100 ng mL^{-1} GFAP (R^2 = 0.998). The limit of

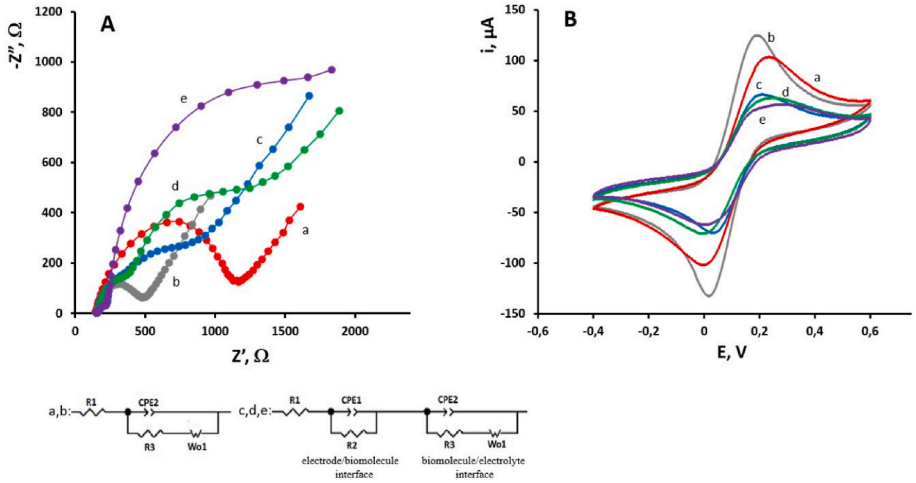

Fig. 6. Nyquist plots (A) and cyclic voltammograms (B) recorded in 5 mM $Fe(CN)_6^{3-/4-}$ in 10 mM PBS of pH 7.4: rGO/MoS_2/AgNPs/SPCE (a, red); rGO/MoS_2/AgNPs/SPCE after treatment with EDC/sulfo-NHS (b, grey); anti-GFAP-rGO/MoS_2/AgNPs/SPCE (c, blue); anti-GFAP-rGO/MoS_2/AgNPs/SPCE after blocking with BB (d, green); GFAP-anti-GFAP-rGO/MoS_2/AgNPs/SPCE (e, dark blue). The equivalent circuits used to adjust the experimental results are shown below.

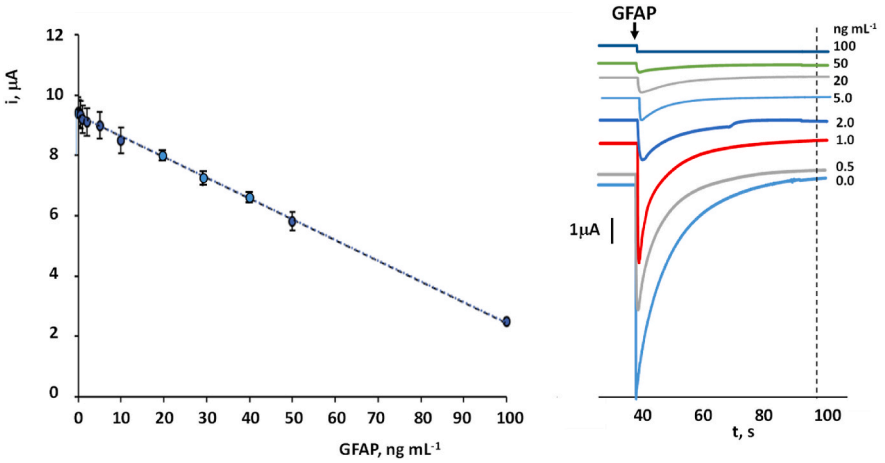

Fig. 7. Calibration plot for the determination of GFAP with the anti-GFAP-rGO/MoS_2/AgNPs/SPCE immunosensor and real amperometric traces recorded for different GFAP concentrations at −0.40 V vs. Ag pseudo-reference electrode. Error bars estimated as triple of the standard deviation ($n = 3$).

detection, LOD = 0.12 ng mL^{-1}, was calculated as the lowest concentration that can be statistically discriminated from zero, according to the $\overline{x}$ + 3s criterion, where s was estimated as the standard deviation (n = 10) for the blank (measurements in the absence of GFAP) in concentration units (ng mL^{-1}). The limit of quantification achieved, $\overline{x}$ + 10s, was LOQ = 0.56 ng mL^{-1}. Intraday and interday reproducibility was evaluated by measuring the amperometric responses of five different immunosensors prepared on the same day or in different days, respectively, in the absence or in presence of 50 ng mL^{-1} of GFAP. The relative standard deviation (RSD) values were 4.6 and 5.9% (intraday), and 5.1 and 6.4% (interday), respectively. These results demonstrated the acceptable reproducibility of the amperometric measurements also indicating the reliability and reproducibility of the method and the immunosensor preparation. The storage stability of the anti-GFAP-rGO/MoS_2/AgNPs/SPCE was also tested. To do that, different immunoplatforms were prepared on the same day, stored in PBS pH 7.4 at 4 °C, and employed to measure GFAP on different days by incubation each time 50 ng mL^{-1} GFAP according to the procedure described in the Experimental section. The obtained results (Fig. S2 Supplementary Information) allowed deducing that the bioelectrodes were stable for at least 23 days (the longest storage time tested) since the current responses remained inside the $\overline{x} \pm 3s$ limits, where s was the standard deviation of the measurements (n = 10) carried out on the first day. Therefore, during this period it is feasible to prepare the immunosensors from the stored bioconjugates, which allows that the determination of GFAP can be accomplished after the protein incubation step which required only 90 min.

When the analytical characteristics exhibited by the developed immunosensor were compared with those claimed for commercial ELISA kits using similar immunoreagents, some noticeable differences are apparent. These kits provide dynamic ranges and quantification limits like those obtained with the immunosensor, although a semilogarithmic relationship between the analytical response and GFAP concentration was obtained with some of the kits such as Mybiosource ELISA kit Nº MBS704044 [www.mybiosource.com/gfap-human-elisa-kits/glial-fibrillary-acidic-protein/704044]. or R&D Systems ELISA kit Nº DY259405 [www.rndsystems.com/products/human-gfap-duoset-elisa_dy2594-05]. Furthermore, immobilization at 37 °C was required with the ELISA tests, whereas all the steps involved in the immunosensor preparation once anti-GFAP was immobilized were performed at room temperature. In addition, the assay time with ELISAs varies from 3 h 30 min to around 4 h 40 min, which is much longer than 2 h 30 min needed with the immunosensor (counting, in both cases, since the immobilization of the capture antibody). Regarding the comparison with the reported biosensors, the magnetically assisted bioplatform described by Ozcelikay et al. [10] provided a calibration plot with a shorter linear

range (up to 31.6 ng mL^{-1}) and required a longer assay time (3 h) than the developed label-free immunosensor. Furthermore, the reported immunosensors using label-free EIS measurements achieved lower LOD values but involved semi-logarithmic calibrations, with shorter assay-time. However, it is important to note that none of these methods were applied to the determination of endogenous GFAP in real samples.

3.3.1. Selectivity

The effect of potential interfering compounds that may be present together with the target biomarker in biological samples on the electrochemical responses obtained with the immunosensor was studied. The compounds tested were proteins related to inflammation and neurological disorders, as well as others usually present in human serum, whose influence was evaluated at concentrations that correspond approximately to the normal physiological level found in healthy individuals: 130 ng mL^{-1} β-chemokine ligand 5 (CCL5); 100 pg mL^{-1} interleukin 6 (IL-6); 100 pg mL^{-1} interferon gamma (INF-γ); 200 pg mL^{-1} tumor necrosis factor alpha (TNF); 1 ng mL^{-1} neurofilament light chain (NfL); 100 μg mL^{-1} uric acid (UA); 5 mg mL^{-1} hemoglobin (HB), and 50 mg mL^{-1} human serum albumin (HSA). The results obtained (Fig. S3 Supplementary Information) show as no significantly different responses were obtained in all cases since all mean steady state current values measured were within the ±3 × standard deviation range of the current values obtained in the absence of potential interferent. This excellent selectivity can be attributed to the practical specificity of the capture antibodies towards the target protein. Furthermore, it should be noticed that no apparent interference was observed for the electroactive uric acid, probably due to the detection potential value selected to monitor the immunosensing event at the modified electrode.

3.4. Determination of GFAP in human cerebrospinal fluid

The usefulness of the developed immunosensor was evaluated by analyzing CSF samples of patients diagnosed with encephalitis. As it is described in Section 2.3, the determination of GFAP was performed by incubating 5 μL of sample and 45 μL of 100 mM PBS pH 6.8 onto the surface of the anti-GFAP-rGO/MoS_2/AgNPs/SPCE followed by amperometric detection at −0.40 V vs Ag pseudo-reference electrode. Once the background current was stabilized, 5 μL of a 50 mM H_2O_2 solution prepared in the same buffer were added and the current generated by the electrochemical reduction of the redox probe at the electrode surface was measured. Considering the linear range of the calibration plot for GFAP standards (Fig. 7) and the low expected concentration of endogenous protein, the determination was carried out with undiluted samples. Furthermore, since CSF from a healthy individual was not available, the calibration plot slope values was compared with the slope resulting from the calibration graph constructed through the additions of GFAP standards over the 0–20 ng mL^{-1} concentration range, to artificial CSF. The obtained value, −0.064 ± 0.001 μA ng^{-1} mL, was very similar to that of the calibration graph constructed with standards (−0.069 ± 0.001 μA ng^{-1} mL). Indeed, the Student's *t*-test provided a value of $t_{exp} = 0.735 < t_{tab} = 2.776$, indicating that no apparent differences between both matrices occurred under the experimental conditions used. Therefore, the concentration of endogenous GFAP in the CSF of encephalitis patients was quantified from a simple interpolation of the responses obtained for the samples into the calibration prepared with artificial CSF. Using this protocol, the obtained results are summarized in Table 2. In addition, these results were compared with those provided by an ELISA method to 20-fold diluted CSF samples involving a sandwich-type configuration. The statistical comparison (t_{exp} was in all cases lower than $t_{tab} = 2.776$) confirmed that similar results were obtained using both methodologies. Furthermore, a correlation graph between the results obtained by both techniques provided a linear graph with $R^2 = 0.994$, slope = 0.97 ± 0.04 and intercept = 1 ± 1, thus confirming the agreement of the results.

Table 2
GFAP concentrations in CSF samples of encephalitis patients obtained with the developed immunosensor and the comparison with those obtained by an ELISA method using the same immunoreagents.

SAMPLE	GFAP, ng mL^{-1}	
	Immunosensor	ELISA
6641	3 ± 3	6 ± 4
8570	32 ± 2	38 ± 6
5195	27 ± 3	27 ± 4

4. Conclusions

In this work, a label-free electrochemical immunosensor for the sensitive determination of GFAP in clinical samples is reported. The methodology involved covalent immobilization of the specific capture antibodies onto screen-printed carbon electrodes modified with rGO/MoS_2/AgNPs nanocomposites and amperometric detection of the electrochemical reduction of H_2O_2 used as the redox probe. The developed immunosensor exhibits high selectivity and reproducibility and has demonstrated its analytical suitability for application to the determination of GFAP biomarker in real CSF samples from patients diagnosed with encephalitis, providing results in agreement with those obtained by applying an ELISA method using the same immunoreagents. It should be highlighted the simplicity and reduced assay time of the method, which make the immunosensing device very promising for use by low-skilled personnel in decentralized settings.

CRediT authorship contribution statement

Lorena García-Rodrigo: Investigation, Validation, Visualization. **Claudia Ramos-López:** Investigation, Validation, Visualization. **Esther Sánchez-Tirado:** Conceptualization, Investigation, Methodology, Validation, Visualization. **Lourdes Agüí:** Conceptualization, Investigation, Methodology, Supervision, Visualization. **Araceli González-Cortés:** Conceptualization, Data curation, Investigation, Project administration, Supervision, Writing - review & editing. **Paloma Yáñez-Sedeño:** Conceptualization, Funding acquisition, Methodology, Supervision, Writing - original draft, Writing - review & editing. **José M. Pingarrón:** Conceptualization, Supervision, Writing - review & editing.

Declaration of competing interest

The authors declare that they have no known competing financial interests or personal relationships that could have appeared to influence the work reported in this paper.

Data availability

Data will be made available on request.

Acknowledgements

The financial support of PID2021-122457OB-I00 (Spanish Ministerio de Ciencia e Innovacion) and the TRANSNANOAVANSENS-CM Program from the Comunidad de Madrid (Grant S2018/NMT-4349) are gratefully acknowledged.

Appendix A. Supplementary data

Supplementary data to this article can be found online at https://doi.org/10.1016/j.talanta.2023.125597.

References

[1] J. Middeldorp, E.M. Hol, GFAP in health and disease, Prog. Neurobiol. 93 (2011) 421–443.

[2] A. Abdelhak, M. Foschi, S. Abu-Rumeileh, J.K. Yue, L. D'Anna, A. Huss, P. Oeckl, A. C. Ludolph, J. Kuhle, A. Petzold, G.T. Manley, A.J. Green, M. Otto, H. Tumani, Blood GFAP as an emerging biomarker in brain and spinal cord disorders, Nat. Rev. Neurosci. 18 (2022) 158–172.

[3] L. Simani, M. Elmi, M. Asadollahi, Serum GFAP level: a novel adjunctive diagnostic test in differentiate epileptic seizures from psychogenic attacks, Seizure 61 (2018) 41–44.

[4] A. Abdelhak, A. Huss, J. Kassubek, H. Tumani, M. Otto, Serum GFAP as a biomarker for disease severity in multiple sclerosis, Sci. Rep. 8 (2018), 14798.

[5] M. Studahl, L. Rosengren, G. Günther, L. Hagberg, Difference in pathogenesis between herpes simplex virus type 1 encephalitis and tick-borne encephalitis demonstrated by means of cerebrospinal fluid markers of glial and neuronal destruction, J. Neurol. 247 (2000) 636–642.

[6] S. Khetani, V. Ozhukil Kollath, V. Kundra, M.D. Nguyen, C. Debert, A. Sen, K. Karan, A. Sanati-Nezhad, Polyethylenimine modified graphene-oxide electrochemical immunosensor for the detection of Glial Fibrillary Acidic Protein in central nervous system injury, ACS Sens. 3 (2018) 844–851.

[7] R. Salahandish, F. Haghayegh, S. Khetani, M. Hassani, A. Sanati-Nezhad, Immuno-affinity potent strip with pre-embedded intermixed PEDOT:PSS conductive polymers and graphene nanosheets for bio-ready electrochemical biosensing of central nervous system injury biomarkers, ACS Appl. Mater. Interfaces 14 (2022) 28651–28662.

[8] M. Mehmandoust, E. Ecehan Erk, M. Soylak, N. Erk, F. Karimi, Metal−organic framework based electrochemical immunosensor for label-free detection of glial fibrillary acidic protein as a biomarker, Ind. Eng. Chem. Res. 62 (2023) 4532–4539.

[9] G. Ozcelikay, F. Mollarasouli, M. Altay Unal, K. Gucuyener, S.A. Ozkan, Ultrasensitive determination of glial-fibrillary-acidic-protein (GFAP) in human serum-matrix with a label-free impedimetric immunosensor, Biosensors 12 (2022) 1165.

[10] G. Ozcelikay, M. Gamella, M. Altay Unal, K. Gucuyener, A. Montero-Calle, R. Barderas, J.M. Pingarrón, S. Campuzano, S.A. Ozkan, Assisting dementia diagnosis through the electrochemical immunosensing of glial fibrillary acidic protein, Talanta 246 (2022), 123526.

[11] C. Kokkinos, A. Economou, M.I. Prodromidis, Electrochemical immunosensors: critical survey of different architectures and transduction strategies Trends, Anal. Chem. 79 (2016) 88–105.

[12] M.I. Prodromidis, Impedimetric immunosensors—a review, Electrochim. Acta 55 (2010) 4227–4233.

[13] T. Wang, H. Zhu, J. Zhuo, Z. Zhu, P. Papakonstantinou, G. Lubarsky, J. Lin, M. Li, Biosensor based on ultrasmall MoS_2 nanoparticles for electrochemical detection of H_2O_2 released by cells at the nanomolar level, Anal. Chem. 85 (2013) 10289–10295.

[14] K.K. Zadeh, J. Ou, Biosensors based on two-dimensional MoS_2, ACS Sens. 1 (1) (2016) 5–16.

[15] Y. Shu, W. Zhang, H. Cai, Y. Yang, X. Yu, Q. Gao, Expanding interlayers of molybdenum disulfide toward highly sensitive sensing of hydrogen peroxide, Nanoscale 11 (2019) 6644–6653.

[16] K. Yadav, D. Verma, G.B.V.S. Laksmi, S. Eremin, P.R. Solanki, Fabrication of label-free and ultrasensitive electrochemical immunosensor based on molybdenum disulfide nanoparticles modified disposable ITO: an analytical platform for antibiotic detection in food samples, Food Chem. 163 (2021), 130245.

[17] S. Kaushik, U.K. Tiwari, S.S. Pal, R.K. Sinha, Rapid detection of *Escherichia coli* using fiber optic surface plasmon resonance immunosensor based on biofunctionalized Molybdenum disulfide (MoS_2) nanosheets, Biosens. Bioelectron. 126 (2019) 501–509.

[18] G. Kaur, S. Sharma, S. Singh, N. Bhardwaj, A. Deep, Selective and sensitive electrochemical sensor for Aflatoxin M1 with a molybdenum disulfide quantum dot/metal–organic framework nanocomposite, ACS Omega 7 (2022) 17600–17608.

[19] M. Khan, A. Bin Yousaf, M. Chen, C. Wei, X. Wu, N. Huang, Z. Qi, L. Li, Molybdenum sulfide/graphene-carbon nanotube nanocomposite material for electrocatalytic applications in hydrogen evolution reactions, Nano Res. 9 (2016) 837–848.

[20] Y. Wang, Y. Wang, D. Wu, H. Ma, Y. Zhang, D. Fan, X. Pang, B. Du, Q. Wei, Label-free electrochemical immunosensor based on flower-like Ag/MoS_2/rGO nanocomposites for ultrasensitive detection of carcinoembryonic antigen, Sens. Actuators, B 255 (2018) 125–132.

[21] M. Vasudevan, S. Remesh, V. Perumal, P. Bothi Raja, M.N.M. Ibrahim, C. B. Gopinath, S. Karuppanan, M. Ovinis, Facile synthesis of MoS_2 nanoflower-Ag NPs grown on lignin-derived graphene for Troponin I aptasensing, Chem. Eng. J. 468 (2023), 143613.

[22] F. Li, L. Zhang, J. Li, X. Lin, X. Li, Y. Fang, J. Huang, W. Li, M. Tian, J. Jin, R. Li, Synthesis of Cu-MoS_2/rGO hybrid as non-noble metal electrocatalysts for the hydrogen evolution reaction, J. Power Sources 292 (2015) 15–22.

[23] Y. Wan, Z. Guo, X. Jiang, K. Fang, X. Lu, Y. Zhang, N. Gu, Quasi-spherical silver nanoparticles: aqueous synthesis and size control by the seed-mediated Lee-Meisel method, J. Colloid Interface Sci. 394 (2012) 263–268.

[24] X. Cai, E.E.L. Tanner, C. Lin, K. Ngamchuea, J.S. Foord, R.G. Compton, The mechanism of electrochemical reduction of hydrogen peroxide on silver nanoparticles, Phys. Chem. Chem. Phys. 20 (2018) 1608–1614.

[25] H. Song, A. Tang, G. Xu, L. Liu, M. Yin, Y. Pan, One-step convenient hydrothermal synthesis of MoS_2/rGO as a high-performance anode for sodium-ion batteries, Int. J. Electrochem. Sci. 13 (2018) 4720–4730.

[26] B. Arévalo, M. Blázquez-García, A. Valverde, V. Serafín, A. Montero-Calle, G. Solís-Fernández, R. Barderas, S. Campuzano, P. Yáñez-Sedeño, J.M. Pingarrón, Binary MoS_2 nanostructures as nanocarriers for amplification in multiplexed electrochemical immunosensing: simultaneous determination of B cell activation factor and proliferation-induced signal immunity-related cytokines, Microchim. Acta 189 (2022) 143.

[27] V.S. Haritha, A. Vijayan, S.R.S. Kumar, R.B. Rakhi, Voltammetric determination of hydrogen peroxide using MoS_2 modified glassy carbon electrodes, Mater. Lett. 301 (2021), 130258.

[28] A. Chrouda, A. Sbartai, F. Bessueille, L. Renaud, A. Maaref, N. Jaffrezic-Renault, Electrically addressable deposition of diazonium-functionalized antibodies on boron-doped diamond microcells for the detection of ochratoxin A, Anal. Methods 7 (2015) 2444–2451.

[29] M. Lian, Y. Shi, L. Chen, Y. Qin, W. Zhang, J. Zhao, D. Chen, Cell membrane and V_2CMXene-based electrochemical immunosensor with enhanced antifouling capability for detection of CD44, ACS Sens. 7 (2022) 2701–2709.

[30] A. Kaur, S. Rana, A. Bharti, A.G. Ram Chaudhary, N. Prabhakar, Voltammetric detection of vitamin D employing Au-MoS_2 hybrid as immunosensing platform, Microchim. Acta 188 (2021) 222.

[31] Z.O. Uygun, H.D. Ertuğrul Uygun, A short footnote: circuit design for faradaic impedimetric sensors and biosensors, Sensor. Actuator. B Chem. 202 (2014) 448–453.